nature neuroscience

Learning enhances the relative impact of top-down processing in the visual cortex

Hiroshi Makino[1] & Takaki Komiyama[1,2]

Theories have proposed that, in sensory cortices, learning can enhance top-down modulation by higher brain areas while reducing bottom-up sensory drives. To address circuit mechanisms underlying this process, we examined the activity of layer 2/3 (L2/3) excitatory neurons in the mouse primary visual cortex (V1) as well as L4 excitatory neurons, the main bottom-up source, and long-range top-down projections from the retrosplenial cortex (RSC) during associative learning over days using chronic two-photon calcium imaging. During learning, L4 responses gradually weakened, whereas RSC inputs became stronger. Furthermore, L2/3 acquired a ramp-up response temporal profile, potentially encoding the timing of the associated event, which coincided with a similar change in RSC inputs. Learning also reduced the activity of somatostatin-expressing inhibitory neurons (SOM-INs) in V1 that could potentially gate top-down inputs. Finally, RSC inactivation or SOM-IN activation was sufficient to partially reverse the learning-induced changes in L2/3. Together, these results reveal a learning-dependent dynamic shift in the balance between bottom-up and top-down information streams and uncover a role of SOM-INs in controlling this process.

The activity of sensory brain areas is determined not only by feedforward sensory inputs (bottom-up), but also by feedback modulation from higher brain areas (top-down)[1–7]. Theories have proposed a learning-related dynamic shift in the balance between bottom-up and top-down information streams, possibly contributing to the formation of internal models to predict and efficiently encode the sensory environment[8–13]. In this framework, sensory processing is thought to be dominated by the bottom-up pathway in the naive condition, faithfully representing the sensory environment. Experience and learning, however, leads to the generation of an internal model that provides top-down predictions in response to sensory inputs. Any mismatch between the top-down prediction and sensory inputs creates a bottom-up prediction error signal propagating forward in the hierarchy, which in turn updates the internal model so that it can better predict future events. Such refined predictive models can then reduce the error signal by suppressing bottom-up processing. Essentially, the brain is a prediction machine that attempts to minimize bottom-up prediction errors (or surprises) by maximizing the accuracy of top-down predictions through learning. Although this notion has substantial intellectual appeal, the circuit mechanisms underlying such a learning-induced shift in the balance of bottom-up and top-down pathways are poorly understood.

A core feature of the cortical circuit is its layered structures embedded in a hierarchical organization[14,15]. In each sensory cortex, L2/3 excitatory neurons receive bottom-up sensory information from excitatory neurons in L4, the main thalamorecipient layer, which generally target perisomatic dendrites of L2/3 neurons[16]. L2/3 neurons also receive top-down inputs at their distal dendrites in L1 from higher cortical areas[17,18]. Interactions between these distinct inputs define the L2/3 activity, which then propagates to higher brain areas. Despite this anatomical information, the manner in which the dynamics of different circuit components may change during learning remains largely unknown. Based on the theoretical framework described above, we hypothesized that the bottom-up pathway is relatively strong in a naive state, reflected by higher L4 activity, and sensory experience and learning enhance the relative effect of the top-down processing to modulate L2/3 (**Fig. 1a**).

To test this hypothesis, we examined the plasticity of the three excitatory circuit components (L2/3 excitatory neurons, L4 excitatory neurons and top-down inputs arriving in L1) in V1 using two-photon calcium imaging during two experience procedures, a visually guided active avoidance task and passive experience, over days. As a source of top-down inputs to V1, we focused on the RSC, which integrates inputs from multiple higher brain areas such as the frontal cortex and hippocampus and sends the densest feedback projections to V1 among non-visual areas[18,19]. RSC has also been suggested to be essential for adaptive behaviors such as visually cued active avoidance[19,20]. During passive sensory experience and associative learning, bottom-up L4 responses gradually reduced, whereas RSC inputs enhanced their activity. The temporal profile of L2/3 responses appeared to be faithful to the visual stimulus in the naive state and remained so during passive sensory experience. With learning, however, L2/3 acquired a ramp-up response profile, with the peak coinciding with the timing of the associated event. This learning-specific change was present in RSC inputs, but not in L4. Moreover, among genetically defined subtypes of inhibitory interneurons, we found a learning-specific reduction in the activity of SOM-INs that mainly inhibit distal dendrites of excitatory neurons at L1 and potentially gate top-down inputs[21,22]. RSC inactivation or SOM-IN activation after learning was sufficient to reverse the learning-induced changes in L2/3 responses. Our results reveal circuit mechanisms

[1]Neurobiology Section, Center for Neural Circuits and Behavior, and Department of Neurosciences, University of California, San Diego, La Jolla, California, USA. [2]JST, PRESTO, University of California, San Diego, La Jolla, California, USA. Correspondence should be addressed to T.K. (tkomiyama@ucsd.edu).

Received 18 May; accepted 15 June; published online 13 July 2015; corrected online 16 July 2015 (details online); doi:10.1038/nn.4061

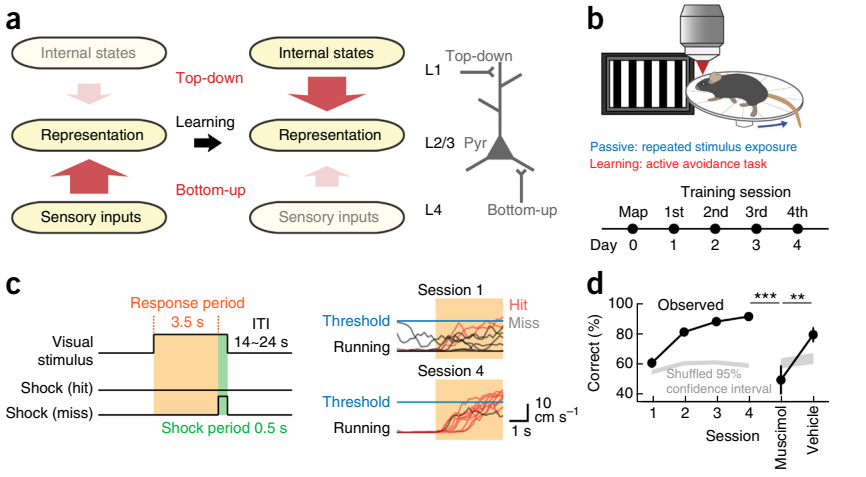

Figure 1 Hypothesis and behavioral procedure. (**a**) Hypothesis. Bottom-up inputs dominate in the naive condition, and learning induces a top-down dominant state. We focused on V1 L2/3 as a potential site subject to such changes. (**b**) Top, schematic of the behavioral setup. Bottom, timeline of the experiment. (**c**) Left, structure of the visually guided active avoidance task. During the first 3.5 s of the visual stimulus (response period), the mouse had to initiate running to avoid a tail shock. Right, example running traces of a mouse in sessions 1 and 4 (ten example trials in each session). (**d**) Behavioral performance improved with training ($P < 0.001$, Kruskal-Wallis test, $n = 47$ mice). Muscimol injections in V1 after learning impaired the performance (***$P < 0.001$, **$P = 0.0016$, one-tailed bootstrap with Bonferroni correction, $n = 7$ mice). Error bars represent s.e.m.

underlying the theoretical postulate of a learning-dependent dynamic shift in the balance between the bottom-up and top-down information streams, involving intricate interactions between long-range intercortical projections and local microcircuits.

RESULTS

Visually guided active avoidance task

To determine the effect of visual experience on V1 processing, we monitored the dynamics of distinct circuit components using chronic two-photon calcium imaging in head-fixed mice[23] on a circular treadmill during visual experience over days. On the first day (day 0), we measured tuning properties of the individual regions of interest (ROIs, cell bodies or axonal boutons) by presenting different directions of drifting gratings (12 directions, 30 degrees apart) and defined their responses as pre-experience activity (naive; **Supplementary Fig. 1**). We then selected one of the directions of drifting gratings as the target stimulus and repeatedly presented it from the next day while monitoring the activity of the same set of ROIs throughout experience (4 s per trial, ~90 trials per 30 min per d for 4 d). In one experience condition (passive), mice passively viewed the same stimulus for 4 d while locomotion was unconstrained. In another condition (learning), mice experienced the same stimulus the same number of times, but in a newly developed visually guided active avoidance task (**Fig. 1b**). In this task, mice were required to detect the visual stimulus and initiate running on the treadmill above the set threshold. The failure to initiate running (that is, no running or continuous running from the pre-stimulus period) during the response period (3.5 s from the visual stimulus onset) was scored as an incorrect trial (miss) and triggered a mild tail shock (0.5 s, 0.6 mA) (**Fig. 1c**). Mice showed efficient learning, with the average correct rate reaching 91 ± 1% at the fourth session ($P < 0.001$, Kruskal-Wallis test, $n = 47$; **Fig. 1d**). Silencing V1 after learning with muscimol, a GABA receptor agonist, impaired the task performance without a noticeable motor deficit (muscimol: $P < 0.001$ versus session 4; vehicle: $P = 0.0016$ versus muscimol, one-tailed bootstrap with Bonferroni correction, $n = 7$; **Fig. 1d**), demonstrating the involvement of V1 in this behavior[24].

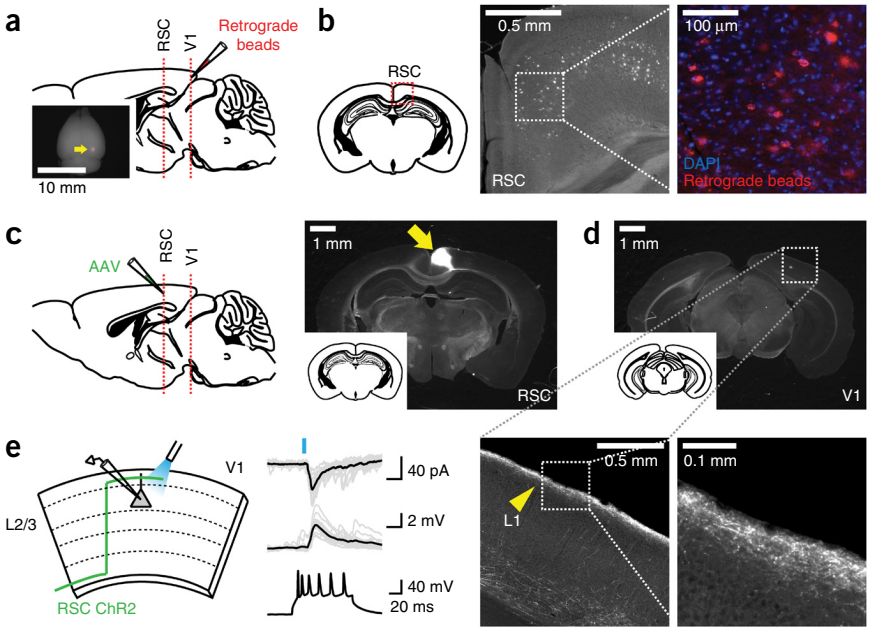

Figure 2 RSC provides monosynaptic excitatory inputs to V1 L2/3 excitatory neurons. (**a**) Retrograde tracing. Retrograde beads were injected into V1 to identify potential brain regions providing top-down inputs ($n = 4$ mice). Inset, injection site indicated by the arrow. (**b**) Left, schematic illustrating the location of RSC. Middle, RSC containing dense labeling of the beads. Right, magnification of the outlined area. Other brain areas labeled with the retrograde beads include anterior cingulate cortex, secondary motor cortex, secondary visual cortex, auditory cortex and lateral geniculate nucleus. RSC was one of the most densely labeled areas. (**c**) Anterograde tracing. AAV expressing ChR2 or GCaMP6f was injected into RSC. Arrow, injection site at RSC. (**d**) GCaMP6f-expressing axons of RSC neurons innervated predominantly in L1 of V1. Bottom left, magnification of the outlined area in V1. Bottom right, magnification of the outlined area in the left panel. Arrowhead, RSC axons arriving in L1 of V1. (**e**) Photoactivation of RSC axons and whole-cell recordings in acute V1 slices revealed monosynaptic excitatory input from RSC to V1 L2/3 excitatory neurons. Traces were light-evoked excitatory postsynaptic currents (top), excitatory postsynaptic potentials (middle) and the regular spiking pattern with current injection, confirming that they were excitatory neurons (bottom). 12 of 13 neurons showed such postsynaptic responses.

Identification of top-down inputs to V1

To monitor the plasticity of each excitatory circuit component during learning, we first identified brain regions providing top-down inputs to V1 by tracing experiments. Retrograde tracing from V1 resulted in dense labeling in RSC among other regions (**Fig. 2a**,**b**), and anterograde tracing from RSC revealed dense axonal projections in L1 of V1 (**Fig. 2c**,**d**). Photoactivation of ChR2-expressing RSC axons in acute V1 slices confirmed monosynaptic excitatory connections on L2/3 excitatory neurons (92%, 12 of 13 L2/3 neurons; **Fig. 2e**). Based on these findings and the importance of RSC for the visually cued active avoidance behavior[20], we focused on RSC as a source of top-down inputs to V1.

Asymmetrical changes in response magnitudes between bottom-up and top-down inputs

We explored the dynamics of the three excitatory components by monitoring the activity of L2/3 excitatory neurons, L4 excitatory neurons or RSC axonal boutons in each mouse throughout the course of the experience procedures (**Fig. 3**). For V1 excitatory neurons, we injected adeno-associated virus (AAV) in V1 to express the genetically encoded calcium indicator GCaMP6f[25]. Excitatory neurons were identified by using transgenic mice expressing tdTomato in all inhibitory neuron types (GAD2-IRES-Cre[26] × Rosa-LSL-tdTomato[27])[28] (Online Methods and **Supplementary Fig. 2**). For RSC inputs, we injected AAV into RSC and imaged the activity of the axonal boutons located in L1 of V1. In both passive and learning conditions, we observed asymmetrical changes in response amplitudes across the three components. The activity of L2/3 and L4 excitatory neurons became sparser over days (**Fig. 3d**–**i**). This was a result of a reduction in the number of responsive neurons while the remaining neurons stably maintained their response magnitude. The reduction in the population response was stimulus specific (**Supplementary Fig. 1**). In stark contrast, RSC inputs substantially enhanced their activity (**Fig. 3a**–**c**). Learning in particular led to a more pronounced increase in RSC input activity compared with passive experience, mainly as a result of an increase in the response amplitudes in each bouton (**Fig. 3c**).

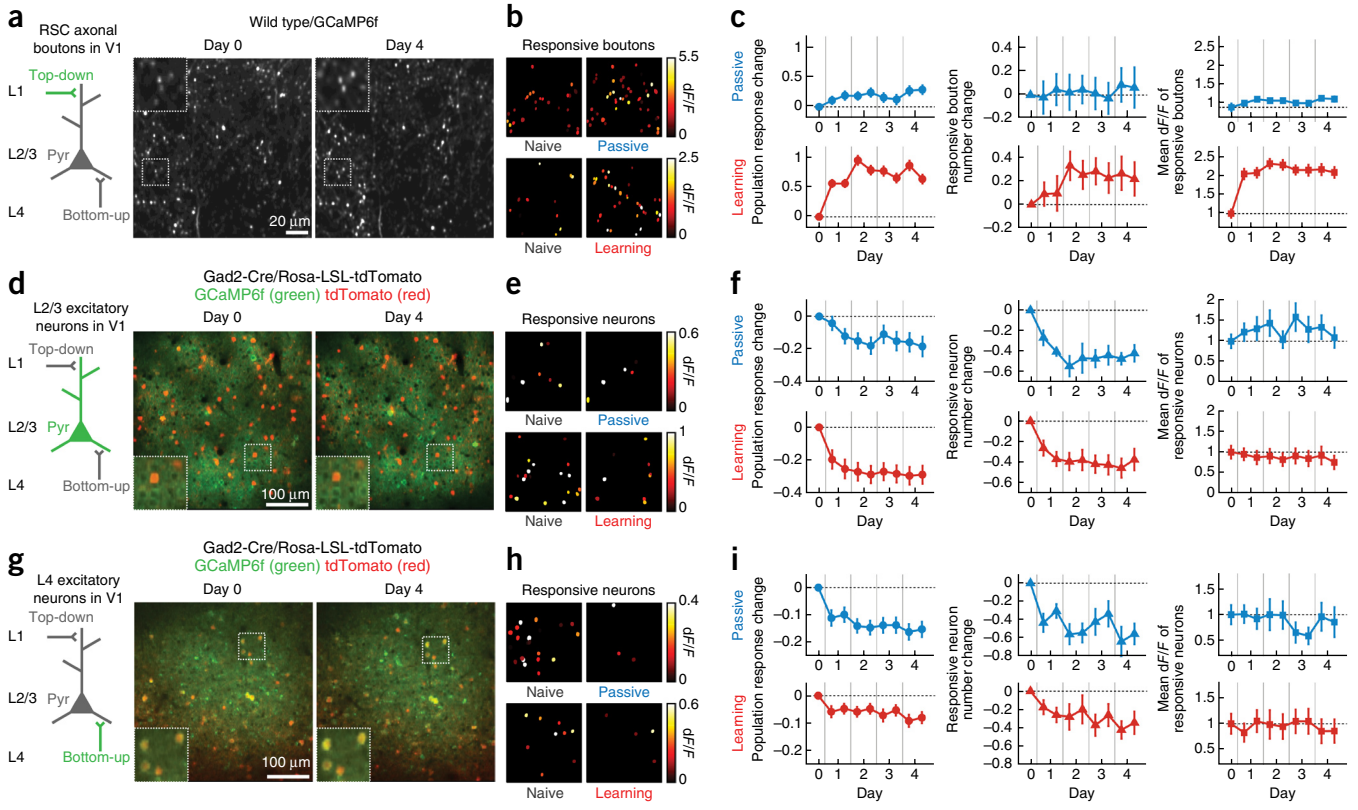

Figure 3 Asymmetrical changes in responses of RSC axons, L2/3 excitatory neurons and L4 excitatory neurons in V1 during passive experience and associative learning. (**a**) Left, circuit schematic with the imaged component (RSC axonal boutons) shown in green. Right, same population of RSC axonal boutons expressing GCaMP6f imaged 4 d apart. Insets are magnifications of outlined areas. (**b**) Spatial map of responsive RSC axonal boutons in an image field from a mouse before (left) and after passive experience or learning (right), pseudocolor-coded according to the activity levels. (**c**) Left, population response change of RSC axonal boutons over days in passive and learning groups. The value at each time point (t) is $R_t - R_0$ where R_0 and R_t are the population response at day 0 and time point t, respectively (defined as the mean dF/F during the stimulus period averaged across trials, and then averaged across all ROIs that were responsive in at least one time point). Each training session (days 1–4) was split into two blocks (passive: $P < 0.001$, $n = 365$ boutons, 6 mice; learning: $P < 0.001$, $n = 227$ boutons, 5 mice; one-way repeated measures ANOVA). Middle, changes in the number of responsive RSC axonal boutons at each time point normalized to the value on day 0 in passive and learning groups (passive: $P = 0.98$, 6 mice; learning: $P = 0.09$, 6 mice; one-way repeated measures ANOVA). Right, dF/F of the RSC axonal boutons that were responsive at each time point in passive and learning groups, normalized to the mean value on day 0 (passive: $P = 0.0051$, 6 mice; learning: $P < 0.001$, 5 mice; Kruskal-Wallis test). (**d**–**f**) Data are presented as in **a**–**c** for L2/3 excitatory neurons. tdTomato in **d** and **g** marks inhibitory neurons. Left in **f**: passive: $P < 0.001$, $n = 88$ neurons, 5 mice; learning: $P < 0.001$, $n = 163$ neurons, 7 mice. Middle in **f**: passive: $P < 0.001$, 5 mice; learning: $P < 0.001$, 7 mice. Right in **f**: passive: $P = 0.22$, 5 mice; learning: $P = 0.57$, 7 mice. (**g**–**i**) Data are presented as in **a**–**c** for L4 excitatory neurons. Left in **i**: passive: $P < 0.001$, $n = 50$ neurons, 5 mice; learning: $P < 0.001$, $n = 81$ neurons, 5 mice. Middle in **i**: passive: $P < 0.001$, 5 mice; learning: $P = 0.03$, 5 mice. Right in **i**: passive: $P = 0.31$, 5 mice; learning: $P = 0.50$, 5 mice. For these and all other analyses, shocked trials (misses) were excluded unless stated otherwise. Error bars represent s.e.m.

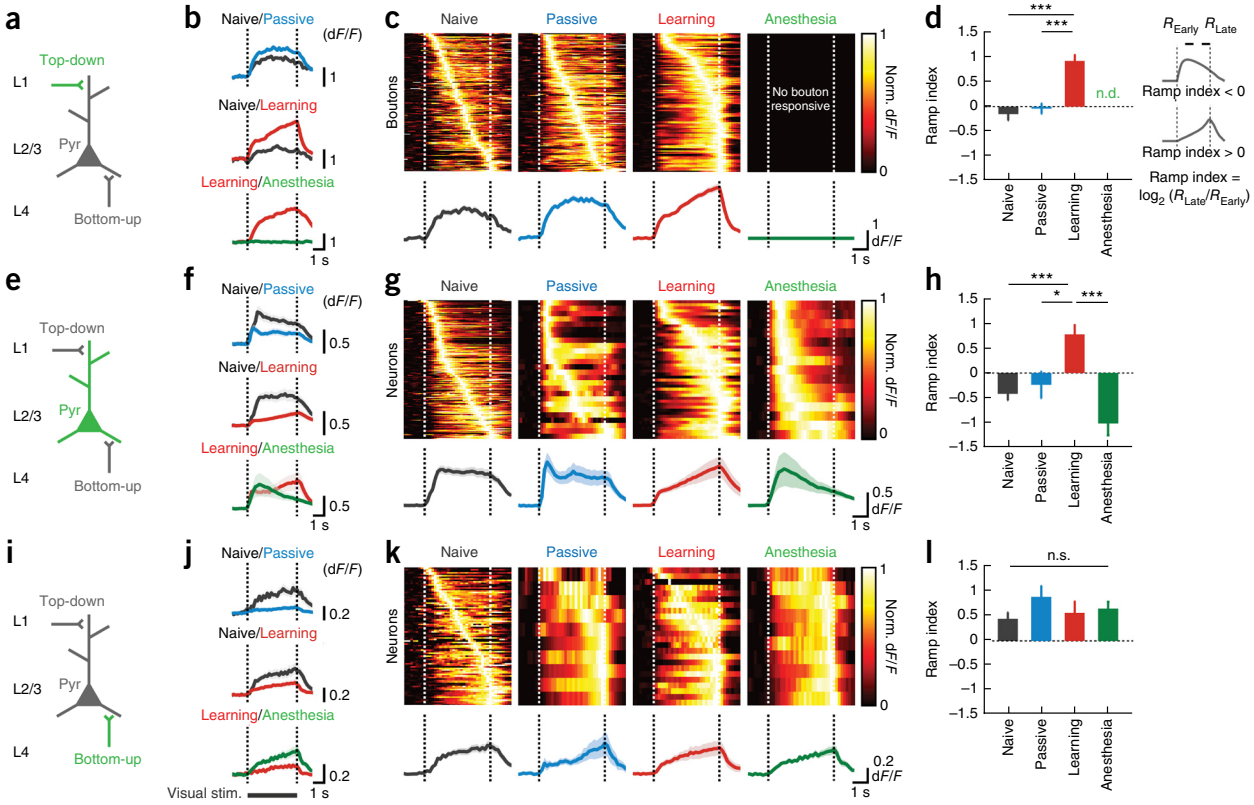

Figure 4 Temporal response patterns of the three excitatory components. (**a**) Circuit schematic with the imaged component (RSC axonal boutons) shown in green. (**b**) Trial-average d*F*/*F* of responsive RSC axonal boutons. Here boutons that were responsive in either of the two conditions are included and each comparison therefore contains the same set of boutons (naive/passive: $n = 236$ boutons, 6 mice; naive/learning: $n = 142$ boutons, 5 mice; learning/post-learning anesthesia, $n = 139$ boutons, 3 mice). (**c**) Top, heat maps of normalized trial-average d*F*/*F* of individual boutons responsive in each time point sorted in the order of peak timing for naive, passive and learning conditions. Bottom, mean d*F*/*F* of the boutons responsive in each time point. Note the emergence of ramp-up responses in RSC inputs and L2/3 excitatory neurons in **g** after learning. Note also that, although the plots in **b**, **f** and **j** include the same set of ROIs for the comparisons, and thus directly reflect the magnitude of population activity, the plots in **c**, **g** and **k** have a varying number of responsive ROIs in each condition and thus focus on the temporal response patterns without faithfully representing the size of population activity. See **Figure 3** for the changes in the number of responsive ROIs. (**d**) Mean ramp index under each condition for RSC axonal boutons (naive: $n = 155$ boutons, 11 mice; passive: 152 boutons, 6 mice; learning: 121 boutons, 6 mice; post-learning anesthesia: 3 mice; $^{***}P < 0.001$, one-way ANOVA with *post hoc* Tukey test). There were no responsive RSC axonal boutons under post-learning anesthesia. All other comparisons in **d**, **h** and **l** were statistically non-significant ($P > 0.05$). (**e**–**h**) Data are presented as in **a**–**d** for L2/3 excitatory neurons (**f**, naive/passive: $n = 71$ neurons, 5 mice; naive/learning: $n = 131$ neurons, 7 mice; learning/post-learning anesthesia: $n = 19$ neurons, 3 mice; **h**, naive: $n = 146$ neurons, 13 mice; passive: 21 neurons, 5 mice; learning: 45 neurons, 7 mice; post-learning anesthesia: 15 neurons, 3 mice; $^{***}P < 0.001$, $^{*}P = 0.038$). (**i**–**l**) Data are presented as in **a**–**d** for L4 excitatory neurons (**j**, naive/passive: $n = 43$ neurons, 5 mice; naive/learning: $n = 55$ neurons, 5 mice; learning/post-learning anesthesia, $n = 13$ neurons, 3 mice; **l**, naive: $n = 72$ neurons, 10 mice; passive: 9 neurons, 5 mice; learning: 23 neurons, 5 mice; post-learning anesthesia: 10 neurons, 3 mice; non-significant, $P = 0.63$).

Learning induces ramp-up responses in L2/3 excitatory neurons and RSC inputs

The asymmetrical changes in L4 and RSC activity provide evidence for an experience-dependent shift of the balance between the top-down and bottom-up streams. To assess the effect of these changes on stimulus representations, we next examined the temporal patterns of the responses of these circuit components (**Fig. 4**). In the naive state, the majority of responsive L2/3 excitatory neurons showed a sharp increase of GCaMP fluorescence at the onset of the visual stimulus, which returned to baseline at stimulus offset. This onset-locked activity persisted in the passive condition over sessions (**Fig. 4e–g** and **Supplementary Fig. 3**). However, after learning, L2/3 excitatory neurons acquired a pattern that gradually ramped up during the stimulus and peaked at the timing of the potential aversive event (**Fig. 4e–g** and **Supplementary Fig. 3**). Such responses may represent an anticipation of the associated event[29] and are reminiscent of a previous study in rats demonstrating that V1 neurons can encode reward timing[30]. To quantify the temporal response profile of individual neurons, we introduced the ramp index, which was $\log_2(R_{Late}/R_{Early})$, where R_{Early} and R_{Late} refer to the activity in the 1–2-s and 3–4-s windows of the stimulus presentation, respectively. The ramp index for L2/3 excitatory neurons was significantly higher in the learning condition compared with the naive and passive groups ($P < 0.001$ versus naive, $P = 0.038$ versus passive, one-way ANOVA with *post hoc* Tukey test; **Fig. 4h** and **Supplementary Fig. 4**). Similar learning-specific changes from onset-locked to ramp-up response patterns were also observed in RSC inputs ($P < 0.001$ versus naive and passive, one-way ANOVA with *post hoc* Tukey test; **Fig. 4a–d** and **Supplementary Fig. 4**). However, the response patterns of L4 excitatory neurons were stable across experience procedures ($P = 0.63$, one-way ANOVA; **Fig. 4i–l** and **Supplementary Fig. 4**). Notably, the changes in the response profile were not a result of changes in the running behavior[31], as the activity was indistinguishable between hit and miss trials (**Supplementary Fig. 5**). In fact, the running-dependent gain modulation[31] was observed in naive and passive conditions, but this effect was eliminated after learning, presumably as a result of occlusion by

learning-dependent changes in top-down processing (**Supplementary Fig. 5**). Moreover, a locomotion-independent learning procedure in another set of mice revealed similar ramp-up response patterns in L2/3 excitatory neurons and the RSC inputs (**Supplementary Fig. 6**). Thus, associative learning induced a ramp-up response pattern in L2/3 and RSC independently of the changes in the running behavior.

RSC is necessary for the expression of L2/3 ramp-up activity

Next we sought to evaluate the possibility that the ramp-up responses in L2/3 excitatory neurons after learning are a result of top-down modulation. First, we asked whether the post-learning responses of L2/3 excitatory neurons require wakefulness, as top-down modulation is considered to be sensitive to brain state[32]. We trained mice for the active avoidance task and then subsequently anesthetized them while following the activity changes in each excitatory circuit component. Anesthesia completely silenced top-down inputs from RSC (**Fig. 4b,c** and **Supplementary Fig. 3**), with little effect on the temporal profile in L4 (**Fig. 4j–l** and **Supplementary Fig. 3**). These changes were accompanied by a restoration of naive-like onset-locked activity in L2/3 excitatory neurons (**Fig. 4f–h** and **Supplementary Fig. 3**). Second, to directly test the requirement of RSC activity for the post-learning responses in L2/3, we inactivated RSC after the behavioral training by muscimol injections (**Fig. 5a**). Consistent with a previous study[20], RSC inactivation impaired the performance of the active avoidance task without noticeable motor impairments (muscimol: $P < 0.001$ versus session 4; vehicle: $P < 0.001$ versus muscimol, one-tailed bootstrap with Bonferroni correction, $n = 9$; **Fig. 5b**). Notably, RSC inactivation after learning restored onset-locked activity in L2/3 excitatory neurons (**Fig. 5c–e**), indicating that RSC activity is necessary for the expression of post-learning L2/3 ramp-up responses. RSC inactivation in the naive state, however, did not change the ramp index of L2/3 excitatory neurons (**Supplementary Fig. 3**). Taken together, these results suggest that learning shifts the balance of bottom-up and top-down drives onto L2/3 excitatory neurons; bottom-up inputs are relatively strong in the naive state, whereas learning enhances the effect of top-down inputs (**Fig. 1a**).

Reduced activity of SOM-INs during learning

How is the effect of these distinct inputs on L2/3 excitatory neurons regulated? It has been suggested that cortical GABAergic interneurons of various types[33–35] can control the flow of information by actively inhibiting distinct subcellular domains of excitatory neurons[36]. In particular, SOM-INs extend their axons to L1 and inhibit the distal dendrites of excitatory neurons, potentially controlling top-down inputs arriving at L1 (refs. 21,22,37). We examined the activity of SOM-INs by injecting AAV encoding Cre-dependent GCaMP6f in SOM-Cre[26] mice (**Fig. 6a**). In the naive state, SOM-INs exhibited responses tuned to stimulus orientation (**Supplementary Fig. 1**), consistent with previous findings[38,39]. Passive experience led to a modest increase in the activity of SOM-INs (**Fig. 6b,c** and **Supplementary Fig. 7**), the magnitude of which was similar to the increase in the RSC axon activity in the same condition (**Fig. 3c**), suggesting that RSC inputs are balanced by SOM-IN inhibition in this context. On the contrary, learning caused a decrease in SOM-IN activity, with fewer SOM-INs responding to the target stimulus (**Fig. 6b,c** and **Supplementary Fig. 7**). Thus, with learning, RSC axon activity increases whereas SOM-IN activity decreases, possibly creating a condition in which RSC inputs exert an even stronger influence on the activity of L2/3 excitatory neurons without being 'gated' by SOM inhibition. SOM-IN activity was suppressed when mice were anesthetized or RSC was inactivated after learning, indicating that RSC is an important driver, either directly or indirectly, of V1 SOM-IN activity (**Supplementary Fig. 7**). With learning, however, the ratio of RSC input activity and SOM-IN activity changed; RSC activity increased, whereas SOM-IN activity decreased. Notably, such learning-specific changes in the visually evoked activity were not observed in parvalbumin (PV) or vasoactive intestinal peptide (VIP)-expressing inhibitory neurons, the two other major subtypes of cortical inhibitory neurons[33,34,36] (**Supplementary Fig. 8**), highlighting the unique position of SOM-INs.

Partial restoration of L2/3 naive-like activity by post-learning SOM-IN reactivation

We addressed whether the reduction in SOM-IN activity is responsible for the expression of the post-learning ramp-up responses of L2/3 excitatory neurons. We manipulated SOM-IN activity, using the stabilized step function opsin (SSFO), which depolarizes a cell for prolonged periods when activated by a brief pulse of blue light until deactivated by amber light[40] (**Supplementary Fig. 9**). Moreover, when PV-INs were activated using SSFO, visually evoked responses of neighboring non-PV neurons monitored by GCaMP6f were significantly and reversibly suppressed ($P < 0.001$; **Supplementary Fig. 9**).

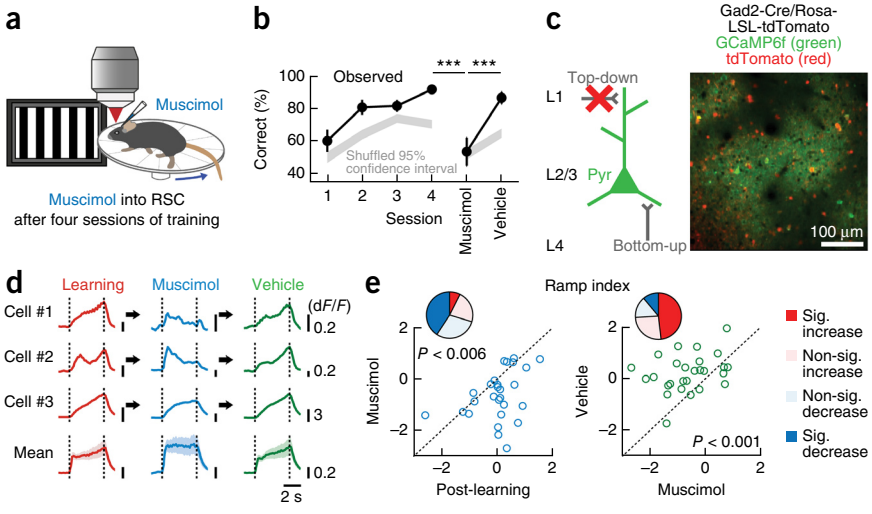

Figure 5 Necessity of RSC for the learned active avoidance behavior and post-learning activity in L2/3 excitatory neurons. (**a**) Schematic of the experiment. (**b**) RSC inactivation impaired the task performance (***$P < 0.001$, one-tailed bootstrap with Bonferroni correction, $n = 9$ mice). (**c**) Monitoring post-learning responses of L2/3 excitatory neurons with RSC inactivation. (**d**) Responses of three example neurons and mean of all responsive neurons showing that RSC inactivation led to more onset-locked responses. For the population mean, all neurons that were responsive in at least one of the three conditions are included. (**e**) Left, ramp index of individual neurons decreased by RSC inactivation after learning ($P = 0.005$, Wilcoxon signed-rank test with Bonferroni correction, $n = 27$ neurons, 7 mice). Right, ramp index was higher with vehicle injections compared with muscimol injections ($P < 0.001$, $n = 27$ neurons, 7 mice). The pie charts illustrate the fractions of neurons showing a significant increase or decrease in the ramp index (Wilcoxon signed-rank test, $P < 0.05$).

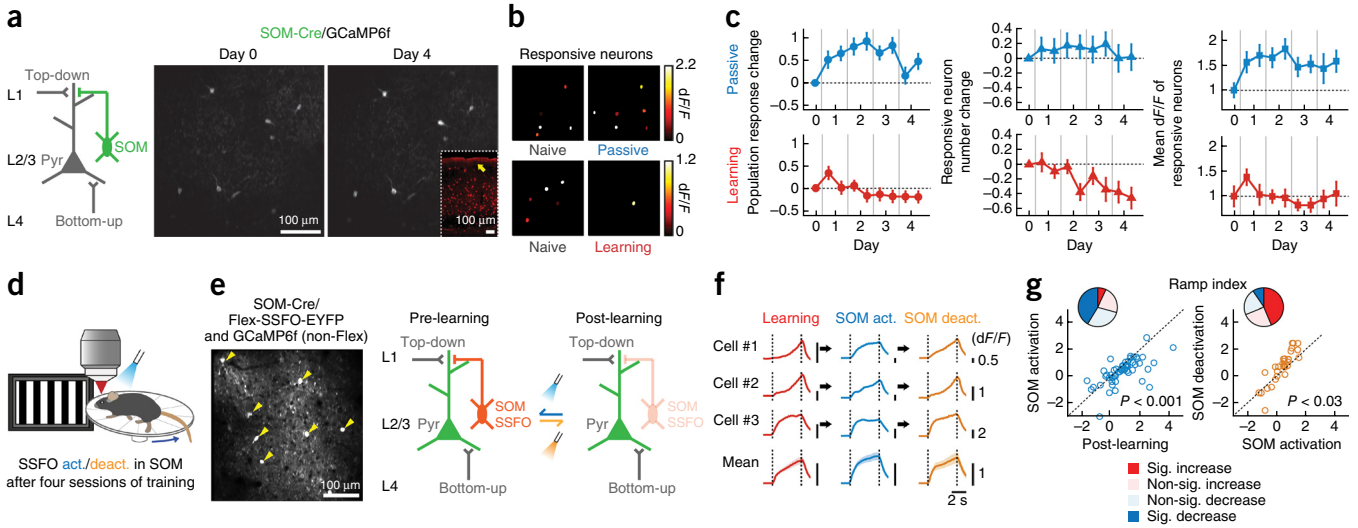

Figure 6 Learning-induced reduction in SOM-IN activity and partial restoration of the naive-like activity in L2/3 by post-learning reactivation of SOM-INs. (**a**) Left, circuit schematic of SOM-IN. Right, same population of SOM-INs expressing GCaMP6f imaged 4 d apart. Inset, coronal section of V1 with tdTomato-expressing SOM-INs. Arrow indicates axons of SOM-INs heavily innervating L1. (**b**) Spatial map of responsive SOM-INs in an image field from a mouse before (left) and after passive experience or learning (right), pseudocolor-coded according to the activity levels. (**c**) Data are presented as in **Figure 3**. Left, population response change (passive: $P < 0.001$, $n = 42$ neurons, 6 mice; learning: $P < 0.001$, $n = 40$ neurons, 7 mice; one-way repeated measures ANOVA). Middle, responsive neuron number change (passive: $P = 0.41$, $n = 7$ mice; learning: $P < 0.001$, $n = 7$ mice; one-way repeated measures ANOVA). Right, mean dF/F of responsive neurons (passive: $P = 0.09$, $n = 7$ mice; learning: $P = 0.24$, $n = 7$ mice; Kruskal-Wallis test). (**d**) Schematic of the SOM-IN reactivation experiment. (**e**) Left, L2/3 SOM-INs expressing SSFO-EYFP (arrowheads) and putative excitatory neurons expressing GCaMP6f imaged *in vivo*. Right, rationale of the experiment. (**f**) Responses of three example L2/3 putative excitatory neurons and mean of all responsive neurons showing that SOM-IN activation led to more onset-locked responses. For the population mean, all neurons that were responsive in at least one of the three conditions are included. (**g**) Left, ramp index of individual putative excitatory neurons decreased with SOM-IN activation ($P < 0.001$, Wilcoxon signed-rank test with Bonferroni correction, $n = 58$ neurons, 6 mice). Right, reversal in the ramp index of individual neurons by SOM-IN deactivation ($P = 0.024$, $n = 32$ neurons, 4 mice). The pie chart illustrates the fractions of neurons showing a significant increase or decrease in the ramp index. Error bars represent s.e.m.

This ability to manipulate neural activity without a continuous light stimulation facilitated the combination of two-photon calcium imaging and optogenetics.

We injected a mixture of AAVs encoding Cre-dependent SSFO and Cre-independent GCaMP6f in SOM-Cre mice to express SSFO in SOM-INs and monitor the activity of non-SOM (mostly excitatory) L2/3 neurons during learning (**Fig. 6d**,**e**). As expected, the majority of responsive non-SOM neurons in L2/3 showed ramp-up activity after learning. However, activation of SOM-INs after learning caused non-SOM neurons to respond in a more onset-locked manner, partially restoring the pattern seen in the naive condition (**Fig. 6f**,**g**). The activity reverted to the ramp-up pattern when SOM-INs were deactivated (**Fig. 6f**,**g**). Notably, light exposure without SSFO expression did not cause any change in the ramp index (**Supplementary Fig. 9**). These results suggest that SOM-INs have a marked effect on the way L2/3 excitatory neurons are driven, possibly acting as a pathway switch[41]; high SOM-IN activity suppresses top-down inputs and biases toward bottom-up dominance, whereas low SOM-IN activity favors top-down inputs.

DISCUSSION

Each brain area receives inputs from multiple sources carrying a variety of information. It is essential that the weights of these various inputs are appropriately regulated in a context-dependent manner. We used chronic two-photon calcium imaging at cellular and synaptic resolution to study how visual experience shapes distinct inputs to a principal neuron type in the primary visual cortex. This approach revealed an experience-driven enhancement of top-down inputs from RSC and reduction of bottom-up inputs from L4. These changes in inputs interact with local SOM-INs, further modifying the effect of the top-down and bottom-up inputs (**Supplementary Fig. 10**). A result of these changes is a shift in V1 L2/3 from a response that is faithful to the stimulus mainly driven by bottom-up processing in the naive state to an association-based representation resulting from enhanced top-down modulation after learning.

Notably, post-learning RSC inactivation or SOM-IN activation partially restored the naive-like activity of L2/3 excitatory neurons both in response magnitude and temporal dynamics. These manipulations were designed to reduce the effect of top-down modulation. Thus, the enhancement of onset-locked activity of L2/3 excitatory neurons by these manipulations is counterintuitive. However, we note that it has been shown that RSC projects to L6 corticothalamic neurons in V1 (ref. 42), which indirectly inhibit dLGN in thalamus as well as upper layers of V1 (refs. 43,44). Thus, top-down inputs from RSC may have a suppressive effect on bottom-up processing, in addition to their excitatory effect underlying the ramp-up response pattern. Furthermore, a growing body of evidence suggests that SOM-INs inhibit not only excitatory neurons, but also other local inhibitory neurons[45–47]. Such a disinhibitory mechanism[48] could function to enhance bottom-up inputs, in addition to the gating effect of SOM-INs on top-down inputs (**Supplementary Fig. 9**). Taken together, we propose that both RSC and SOM-INs have dual effects on V1 processing: RSC directly excites L2/3 neurons and indirectly inhibits the bottom-up pathway, whereas SOM-INs inhibit distal dendrites of L2/3 neurons to gate top-down inputs and indirectly disinhibit basal dendrites receiving bottom-up inputs. These dual effects may allow them to effectively control the balance of top-down and bottom-up inputs (**Supplementary Fig. 10**). Such potential interactions between top-down and bottom-up inputs

are consistent with the core concept of predictive coding in which top-down predictions could suppress or 'explain away' bottom-up prediction errors[8,10,12]. Furthermore, such learning-related shifts in the neocortical operation mode may be a fundamental feature of cortical computations underlying associative feature binding, with association-based sensory representations, and invariant objection recognition, by effectively ignoring irrelevant fluctuations in sensory inputs resulting from the noise in the sensory environment[49,50]. Our results provide experimental evidence and mechanistic understandings in the V1 microcircuit for these theoretical frameworks.

METHODS

Methods and any associated references are available in the online version of the paper.

Note: Any Supplementary Information and Source Data files are available in the online version of the paper.

ACKNOWLEDGMENTS

We thank A. Kim and L. Xiao for technical assistance, L.L. Looger, J. Akerboom, D.S. Kim and the GENIE Project at Janelia Farm for making GCaMP available, S. Olsen, B. Liu, S. Ruediger-Lee and M. Scanziani for help with visual stimulation and circular treadmill, S. Shabel and R. Malinow for help with slice experiments, and M. Basso, R. Malinow, J. Serences and members of the Komiyama laboratory for comments and discussions. This work was supported by grants from the US National Institutes of Health (1R01NS091010-01, 1R01DC014690-01), Japan Science and Technology Agency (PRESTO), Pew Charitable Trusts, Alfred P. Sloan Foundation, David & Lucile Packard Foundation, Human Frontier Science Program, McKnight Foundation, and the New York Stem Cell Foundation (NYSCF) to T.K. H.M. was supported by the Uehara Memorial Foundation Research Fellowship and the JSPS postdoctoral fellowship for Research Abroad. T.K. is a NYSCF-Robertson Investigator.

AUTHOR CONTRIBUTIONS

H.M. and T.K. conceived the project. H.M. performed the experiments. H.M. and T.K. analyzed the data and wrote the manuscript.

COMPETING FINANCIAL INTERESTS

The authors declare no competing financial interests.

1. Desimone, R. & Duncan, J. Neural mechanisms of selective visual attention. *Annu. Rev. Neurosci.* **18**, 193–222 (1995).
2. Hupé, J.M. *et al.* Cortical feedback improves discrimination between figure and background by V1, V2 and V3 neurons. *Nature* **394**, 784–787 (1998).
3. Engel, A.K., Fries, P. & Singer, W. Dynamic predictions: oscillations and synchrony in top-down processing. *Nat. Rev. Neurosci.* **2**, 704–716 (2001).
4. Krupa, D.J., Wiest, M.C., Shuler, M.G., Laubach, M. & Nicolelis, M.A. Layer-specific somatosensory cortical activation during active tactile discrimination. *Science* **304**, 1989–1992 (2004).
5. Nienborg, H. & Cumming, B.G. Decision-related activity in sensory neurons reflects more than a neuron's causal effect. *Nature* **459**, 89–92 (2009).
6. Gilbert, C.D. & Li, W. Top-down influences on visual processing. *Nat. Rev. Neurosci.* **14**, 350–363 (2013).
7. Harris, K.D. & Mrsic-Flogel, T.D. Cortical connectivity and sensory coding. *Nature* **503**, 51–58 (2013).
8. Rao, R.P. & Ballard, D.H. Predictive coding in the visual cortex: a functional interpretation of some extra-classical receptive-field effects. *Nat. Neurosci.* **2**, 79–87 (1999).
9. Hinton, G.E. Learning multiple layers of representation. *Trends Cogn. Sci.* **11**, 428–434 (2007).
10. Friston, K. The free-energy principle: a unified brain theory? *Nat. Rev. Neurosci.* **11**, 127–138 (2010).
11. Olshausen, B.A. & Field, D.J. Sparse coding of sensory inputs. *Curr. Opin. Neurobiol.* **14**, 481–487 (2004).
12. Bastos, A.M. *et al.* Canonical microcircuits for predictive coding. *Neuron* **76**, 695–711 (2012).
13. Gdalyahu, A. *et al.* Associative fear learning enhances sparse network coding in primary sensory cortex. *Neuron* **75**, 121–132 (2012).
14. Mignard, M. & Malpeli, J.G. Paths of information flow through visual cortex. *Science* **251**, 1249–1251 (1991).
15. Felleman, D.J. & Van Essen, D.C. Distributed hierarchical processing in the primate cerebral cortex. *Cereb. Cortex* **1**, 1–47 (1991).
16. Petreanu, L., Mao, T., Sternson, S.M. & Svoboda, K. The subcellular organization of neocortical excitatory connections. *Nature* **457**, 1142–1145 (2009).
17. Cauller, L.J. & Connors, B.W. Synaptic physiology of horizontal afferents to layer I in slices of rat SI neocortex. *J. Neurosci.* **14**, 751–762 (1994).
18. Zhang, S. *et al.* Selective attention. Long-range and local circuits for top-down modulation of visual cortex processing. *Science* **345**, 660–665 (2014).
19. Vann, S.D., Aggleton, J.P. & Maguire, E.A. What does the retrosplenial cortex do? *Nat. Rev. Neurosci.* **10**, 792–802 (2009).
20. Lukoyanov, N.V. & Lukoyanova, E.A. Retrosplenial cortex lesions impair acquisition of active avoidance while sparing fear-based emotional memory. *Behav. Brain Res.* **173**, 229–236 (2006).
21. Gentet, L.J. *et al.* Unique functional properties of somatostatin-expressing GABAergic neurons in mouse barrel cortex. *Nat. Neurosci.* **15**, 607–612 (2012).
22. Palmer, L., Murayama, M. & Larkum, M. Inhibitory regulation of dendritic activity *in vivo*. *Front. Neural Circuits* **6**, 26 (2012).
23. Dombeck, D.A., Harvey, C.D., Tian, L., Looger, L.L. & Tank, D.W. Functional imaging of hippocampal place cells at cellular resolution during virtual navigation. *Nat. Neurosci.* **13**, 1433–1440 (2010).
24. Glickfeld, L.L., Histed, M.H. & Maunsell, J.H. Mouse primary visual cortex is used to detect both orientation and contrast changes. *J. Neurosci.* **33**, 19416–19422 (2013).
25. Chen, T.W. *et al.* Ultrasensitive fluorescent proteins for imaging neuronal activity. *Nature* **499**, 295–300 (2013).
26. Taniguchi, H. *et al.* A resource of Cre driver lines for genetic targeting of GABAergic neurons in cerebral cortex. *Neuron* **71**, 995–1013 (2011).
27. Madisen, L. *et al.* A robust and high-throughput Cre reporting and characterization system for the whole mouse brain. *Nat. Neurosci.* **13**, 133–140 (2010).
28. Peters, A.J., Chen, S.X. & Komiyama, T. Emergence of reproducible spatiotemporal activity during motor learning. *Nature* **510**, 263–267 (2014).
29. Janssen, P. & Shadlen, M.N. A representation of the hazard rate of elapsed time in macaque area LIP. *Nat. Neurosci.* **8**, 234–241 (2005).
30. Shuler, M.G. & Bear, M.F. Reward timing in the primary visual cortex. *Science* **311**, 1606–1609 (2006).
31. Niell, C.M. & Stryker, M.P. Modulation of visual responses by behavioral state in mouse visual cortex. *Neuron* **65**, 472–479 (2010).
32. Cauller, L. Layer I of primary sensory neocortex: where top-down converges upon bottom-up. *Behav. Brain Res.* **71**, 163–170 (1995).
33. Kawaguchi, Y. & Kubota, Y. GABAergic cell subtypes and their synaptic connections in rat frontal cortex. *Cereb. Cortex* **7**, 476–486 (1997).
34. Markram, H. *et al.* Interneurons of the neocortical inhibitory system. *Nat. Rev. Neurosci.* **5**, 793–807 (2004).
35. Brown, S.P. & Hestrin, S. Cell-type identity: a key to unlocking the function of neocortical circuits. *Curr. Opin. Neurobiol.* **19**, 415–421 (2009).
36. Kepecs, A. & Fishell, G. Interneuron cell types are fit to function. *Nature* **505**, 318–326 (2014).
37. Lovett-Barron, M. *et al.* Dendritic inhibition in the hippocampus supports fear learning. *Science* **343**, 857–863 (2014).
38. Ma, W.P. *et al.* Visual representations by cortical somatostatin inhibitory neurons: selective but with weak and delayed responses. *J. Neurosci.* **30**, 14371–14379 (2010).
39. Kerlin, A.M., Andermann, M.L., Berezovskii, V.K. & Reid, R.C. Broadly tuned response properties of diverse inhibitory neuron subtypes in mouse visual cortex. *Neuron* **67**, 858–871 (2010).
40. Yizhar, O. *et al.* Neocortical excitation/inhibition balance in information processing and social dysfunction. *Nature* **477**, 171–178 (2011).
41. Callaway, E.M. Feedforward, feedback and inhibitory connections in primate visual cortex. *Neural Netw.* **17**, 625–632 (2004).
42. Vélez-Fort, M. *et al.* The stimulus selectivity and connectivity of layer six principal cells reveals cortical microcircuits underlying visual processing. *Neuron* **83**, 1431–1443 (2014).
43. Olsen, S.R., Bortone, D.S., Adesnik, H. & Scanziani, M. Gain control by layer six in cortical circuits of vision. *Nature* **483**, 47–52 (2012).
44. Bortone, D.S., Olsen, S.R. & Scanziani, M. Translaminar inhibitory cells recruited by layer 6 corticothalamic neurons suppress visual cortex. *Neuron* **82**, 474–485 (2014).
45. Cottam, J.C., Smith, S.L. & Hausser, M. Target-specific effects of somatostatin-expressing interneurons on neocortical visual processing. *J. Neurosci.* **33**, 19567–19578 (2013).
46. Pfeffer, C.K., Xue, M., He, M., Huang, Z.J. & Scanziani, M. Inhibition of inhibition in visual cortex: the logic of connections between molecularly distinct interneurons. *Nat. Neurosci.* **16**, 1068–1076 (2013).
47. Xu, H., Jeong, H.Y., Tremblay, R. & Rudy, B. Neocortical somatostatin-expressing GABAergic interneurons disinhibit the thalamorecipient layer 4. *Neuron* **77**, 155–167 (2013).
48. Letzkus, J.J. *et al.* A disinhibitory microcircuit for associative fear learning in the auditory cortex. *Nature* **480**, 331–335 (2011).
49. Deco, G. & Rolls, E.T. A neurodynamical cortical model of visual attention and invariant object recognition. *Vision Res.* **44**, 621–642 (2004).
50. Larkum, M. A cellular mechanism for cortical associations: an organizing principle for the cerebral cortex. *Trends Neurosci.* **36**, 141–151 (2013).

ONLINE METHODS

Animals. All procedures were in accordance with the Institutional Animal Care and Use Committee at University of California, San Diego. Mice were obtained from the Jackson Laboratory (GAD2-Cre [JAX: 010802], Rosa-CAG-LSL-tdTomato [JAX: 007914], SOM-Cre [JAX: 013044], PV-Cre [JAX: 008069], VIP-Cre [JAX: 010908]) and Charles River Laboratory (C57Bl/6 wild type). Mice were group housed (typically 2–4 mice) with a reversed light cycle (12 h:12 h) in standard plastic disposable cages. Mice had no prior history of drug administration or surgery that could affect the results, and were randomly assigned to each experimental group. Experiments were typically performed during the dark period. Only male mice were used for the *in vivo* experiments. Both male and female mice were used for the *in vitro* experiments.

Surgery for *in vivo* imaging experiments. Adult mice (between 6 weeks and 6 months old) were anesthetized with 1–2% isoflurane (vol/vol) and a circular piece of scalp was removed. After cleaning the underlying bone using a razor blade, a custom-built head-post was implanted to the exposed skull with glue and cemented with black dental acrylic (Lang Dental). A craniotomy (~3 mm in diameter) was made over the right V1 (2.5 mm lateral and 0 mm anterior to lambda) and viruses (AAV2/1-Syn-GCaMP5G or AAV2/1-Syn-GCaMP6f for L2/3 excitatory neurons, AAV2/1-Syn-GCaMP6f for L4 excitatory neurons, AAV2/1-Syn-Flex-GCaMP6f for SOM-INs, PV-INs and VIP-INs, and AAV2/1-EF1α-DIO-hChR2(C128S/D156A)-EYFP (stabilized step-function opsin, SSFO) for the SSFO experiment, University of Pennsylvania Vector Core Facility) were injected using a beveled pipette (~20-μm tip in diameter, Drummond Scientific) backfilled with mineral oil at a speed of ~10 nl min^{-1} (~250 μm deep, 5 sites, ~20 nl per site for L2/3 excitatory neurons, SOM-INs, PV-INs and VIP-INs; ~400 μm deep, 5 sites, ~20 nl per site for L4 excitatory neurons; ~150 μm deep, 3 sites, ~60–100 nl per site of a mixture of SSFO and GCaMP6f-expressing viruses for the SSFO experiment). For RSC axonal calcium imaging, a small craniotomy (~0.5 mm in diameter) was made over the right RSC (0.4 mm lateral and 2.4 mm posterior to bregma) for virus injection (AAV2/1-Syn-GCaMP6f, ~350 μm deep, 1 site, ~50 nl, at ~10 nl min^{-1}) and another craniotomy (~3 mm in diameter) for imaging was made over the right V1 area. RSC injection sites were confirmed by histology in all mice after *in vivo* imaging. After each injection, pipettes were left in the brain for an additional ~4 min to prevent backflow. Following virus injections, a chronic imaging window was placed in the craniotomy. The imaging window was constructed from a small glass plug (Fisher Scientific; number 2 thickness, ~3 mm in diameter) attached to a larger glass base (Fisher Scientific; number 1 thickness, ~4 mm in diameter) using a ultraviolet-curing adhesive (Norland Products). 1.5% agarose was applied to fill the gap between the skull and the window and black dental acrylic was placed to secure the window. Black dental acrylic was selected to prevent light entry to the brain from the LCD monitor. General analgesia (buprenorphine, 0.1 mg per kg of body weight) was subcutaneously injected and mice were monitored until they recovered from anesthesia.

Behavior. Mice were accustomed to the training setup and allowed to freely run on a custom-made circular treadmill under head-fixation for a few sessions before the imaging session. More than 2 weeks (14–51 d) after surgery, two-photon calcium imaging was performed while mice were trained with the visually guided active avoidance task. Visual stimuli (full-field square drifting gratings; temporal frequency: 3 Hz, spatial frequency: 0.04 cycles per degree, not corrected for monitor angle, 100% contrast) were generated in Matlab (MathWorks) using the Psychophysics Toolbox[51] and were displayed on a LCD monitor (30 × 38 cm, Dell) positioned 25 cm from the left eye. For mapping of orientation tuning (day 0), stimuli of 12 equally spaced (30°) directions were pseudo-randomly (or sequentially) presented. The duration of the visual stimulus was 4 s and the inter-trial interval (ITI, mean luminance gray screen displayed) was 8 s. For visual experience (passive, learning and conditioning, days 1–4), one of these 12 directions was selected as the target stimulus and presented repeatedly. The target stimulus was chosen randomly out of the orientations that evoked significant responses in the field of view. The duration of the visual stimulus was 4 s and ITIs were varied between 14 and 24 s so that mice could not predict the timing of the subsequent trials. Running was continuously monitored using an optical encoder (US Digital) connected to a data acquisition device (National Instrument) with custom-written software in LabView (National Instrument) and recorded in Matlab (Ephus). Threshold for running during training sessions was set to 17 cm s^{-1}. In the learning condition, if mice initiated running over this threshold during response period (3.5 s from the onset of the visual stimulus), the trial was scored as a correct trial (hit). If mice either continuously ran over the threshold or did not reach the threshold, the trial was scored as an incorrect trial (miss). In such incorrect trials, mice received a mild tail shock (0.6 mA, 0.5 s co-terminating with the visual stimulus) applied through a pair of metal coil springs attached to a stimulus isolator (A.M.P.I.). In the conditioning group, the visual stimulus was presented similarly and mice received a mild tail shock in 80% of randomly selected trials. The shock was not given in the remaining 20% of the trials. The behavioral setup was controlled by software (Dispatcher, Z. Mainen and C. Brody) running on Matlab with a real-time system (RTLinux). Each session lasted approximately 30 min consisting of ~90 trials.

Inactivation with muscimol. To test the requirement of V1 and RSC, either naive mice or adult mice trained for the task for four sessions received muscimol hydrobromide (5 μg $μl^{-1}$, Sigma) injection under anesthesia with 1–1.5% isoflurane with a beveled pipette (~20-μm tip in diameter) through a small craniotomy (~0.5 mm in diameter) (~60 nl at each site at ~20 nl min^{-1}, V1: bilateral injections at 2.5 mm lateral and 0 mm anterior to lambda at the depths of 300 μm and 600 μm from the brain surface; RSC: unilateral injections in 5 sites, from ~600 μm to ~2,000 μm to lambda along the anterior-posterior axis, ~400 μm lateral to the midline, at the depth of 350 μm). Pipettes were left in the brain for additional ~4 min after each injection. After injections, mice recovered from anesthesia in their home cage for 1–1.5 h before behavioral testing or imaging. During testing sessions, mice did not show any obvious motor deficits. Similar injections were made with a vehicle (cortex buffer containing (in mM) 125 NaCl, 5 KCl, 10 glucose, 10 HEPES, 2 $CaCl_2$, 2 $MgSO_4$) on a separate day as a control.

Imaging. Imaging was performed using a commercial two-photon microscope (MOM, Sutter Instrument) with a Ti:Sapphire excitation laser (Mai Tai, Spectra-Physics) tuned to 925 nm. To isolate photons emitted by fluorescent probes from the visual display, the microscope was enclosed with a blackout material (Thorlab). The objective lens (16×, 0.8 NA, Nikon) was also covered with the same material with a small hole, which allowed excitation laser entry and photon emission from the brain. This blackout material was attached to a head-post covered with cement using glue. The optical axis of the objective was adjusted for each mouse to be perpendicular to the imaging window. Mice with excessive brain movement or limited optical access due to bone growth or virus infection were excluded.

Images were acquired using ScanImage[52] at 6.3 Hz, 512 × 128 pixels (420 × 420 μm; for axonal imaging: 170 × 170 μm). Imaging was performed at the depth of 131–249 μm for L2/3 neurons (excitatory, SOM-INs, PV-INs and VIP-INs), 38–78 μm (L1) for RSC axons and 384–420 μm for L4 excitatory neurons. For mapping of orientation tuning, time-series images were collected for ten trials each of which consisted of 1,000 frames. For behavioral training, a total of 12,000 frames (6 sets of 2,000 frames, a few seconds gap between each set) were acquired each session (18,000 frames with 9 sets of 2,000 frames for the SOM-SSFO experiment). Imaging and behavioral data were acquired separately and aligned to each other offline. If there was a trial during the imaging gaps, the trial was excluded from the analysis. Images were continuously monitored throughout the experiment, and slow drifts of the image were manually corrected using a reference image. For each mouse, only one field of view was imaged except the anesthesia and PV-SSFO experiments, in which up to three fields of view were imaged (1 field of view per d).

For the anesthesia experiment, mice were first trained for 4–5 sessions. On the experiment day, the activity of L2/3 excitatory neurons, L4 excitatory neurons, RSC axonal boutons or SOM-INs was imaged in awake mice for ~15 min (corresponding to 6,000 frames) during the active avoidance task before anesthesia. A mixture of ketamine (100–200 mg per kg) and xylazine (8–16 mg per kg) was then injected intraperitoneally into the mice, and imaging was resumed ~30 min later when mice were lightly anesthetized. In a subset of mice, this procedure was repeated over two days in two different fields of view.

***In vivo* photoactivation.** For SSFO activation of SOM-INs, mice were first trained for four sessions. On the experiment day, L2/3 activity was imaged for ~15 min

(corresponding to 6,000 frames) before photoactivation. Imaging was then paused and the objective lens was put aside for the access of an LED fiber optic (1-mm diameter, Doric Lenses). A 470-nm blue light pulse (~60 mW, 5 s) was presented to photoactivate SSFO at ~5 mm from the window. The objective lens was placed back and imaging was resumed. After ~15 min of imaging, a 590-nm amber light pulse (~10 mW, 30 s) was presented similarly and image acquisition was resumed for additional ~15 min.

Data analysis. All analyses were performed using custom codes in Matlab (MathWorks).

To determine chance levels of the task performance, the timing of each trial was shuffled in each session for each mouse and hit rate was calculated in this surrogate data. The hit rates were averaged across all mice for each shuffle. This was repeated 1,000 times to obtain a distribution of the chance performance level.

To correct for brain motion after image acquisition, we used cross correlation-based image alignment (Turboreg[53], ImageJ Plugin), followed by a hidden Markov model-based line-by-line correction algorithm[54]. ROIs corresponding to neuronal cell bodies or axonal boutons were selected manually. Only neurons or axonal boutons that could be identified in every image session were analyzed. Neurons whose nucleus was filled with GCaMP fluorescence or axonal boutons whose shaft had strong GCaMP basal fluorescence at any point during the experiment were excluded from analysis. Pixels in each ROI were averaged to create fluorescence time series. For somatic imaging, background fluorescence fluctuations were subtracted from each ROI trace to remove neuropil contamination as described previously[28]. Briefly, a ring-shaped background ROI was obtained around each neuron. From this background ROI, pixels containing calcium transients that did not contaminate neuronal ROI were excluded and the remaining pixels were averaged, yielding background fluorescence time-series. The time-varying baselines of fluorescence traces for neuronal and background ROIs were estimated as described previously[28]. In brief, inactive portions of the fluorescence time series were chosen and loess smoothed, and the gaps (that is, active portions) were filled by linear interpolation, yielding the baseline fluorescence trace, F. After baseline estimation, ΔF of the background fluorescence trace was subtracted from the neuronal ROI fluorescence trace to obtain background-subtracted fluorescence time-series, and $\Delta F/F$ for the neuronal ROI was obtained from this trace.

Visually responsive ROIs were determined in each trial block (the entire day 0 (tuning mapping) or a half of each of days 1–4) using the following criteria. For each direction of drifting gratings (or target stimulus for training sessions), ROIs were scored as responsive in a given trial if $\Delta F/F$ in at least three image frames (corresponding to ~0.5 s) during the first 3.5 s of the visual stimulus exceeded 4× s.d. (3× s.d. for L4 excitatory neurons, PV-INs and VIP-INs). s.d. was defined using periods when the visual stimulus was off. The last 0.5 s of the visual stimulus period was not considered to identify responsive ROIs in order to avoid the potential ROI activation by the tail shock. If an ROI was active in more than 20% of all trials or 40% of all running trials, the ROI was deemed visually responsive.

For ROIs that are responsive to any of the stimulus directions on day 0, orientation tuning was determined using the average of all ten trials. The orientation selectivity index (OSI) was calculated as 1 − circular variance (V)[55] defined as

$$V = 1 - \left| \frac{\sum_k R_k e^{i2\theta_k}}{\sum_k R_k} \right|$$

where R_k is the mean integrated $\Delta F/F$ area during the visual stimulus in the kth direction, and θ_k is the direction of the visual stimulus in radians. The direction selectivity index (DSI) was calculated as $(R_{prefer} - R_{opposite})/(R_{prefer} + R_{opposite})$, where R_{prefer} is the mean integrated $\Delta F/F$ area during the visual stimulus in the preferred direction and $R_{opposite}$ is the mean integrated $\Delta F/F$ area during the visual stimulus in the opposite direction.

During visual experience, only correct trials were considered unless noted otherwise. In the passive condition, the 'correct' trials corresponded to trials which would be scored as hit in the learning condition (running during the response period). 'Naive' responses were the average response to the target stimulus from running trials on day 0. Post-experience responses were obtained from the average dF/F of correct trials in the second half of the last experience session (day 4). For naive responses in the conditioning group, only non-running trials were considered. Mice in this condition typically did not run during the following sessions (days 1 to 4) and all of the 20% non-shock trials on day 4 were analyzed.

The population activity change at time point t was calculated as the difference in mean dF/F during the visual stimulus on day 0 and time point t for ROIs that were responsive in at least one time point. The responsive ROI number change was obtained as (responsive ROI number at time point t − responsive ROI number on day 0) / (responsive ROI number at time point t + responsive ROI number on day 0). The mean dF/F of responsive ROIs was obtained as the mean dF/F of ROIs that are responsive at the time point t, which was normalized to the mean dF/F of responsive ROIs on day 0.

For the SSFO and anesthesia experiments, the first ten correct trials for each ~15 min trial block were excluded from analysis.

Ramp index was defined as $\log_2(R_{Late}/R_{Early})$ where R_{Early} = mean dF/F between 1–2 s from the visual stimulus onset and R_{Late} = mean dF/F for the last 1 s of the visual stimulus. Neurons or axonal boutons with R_{Early} or R_{Late} below 0, or mean dF/F during the stimulus presentation below 0.02 were excluded for the ramp index measurement. Neurons with significant changes in the ramp index were determined by Wilcoxon signed-rank test with the P value below 0.05.

Error bars indicate s.e.m. and statistics were performed with two-tailed tests unless noted otherwise. For bootstrap tests, 10,000 repetitions were performed. No statistical methods were used to predetermine sample sizes, but our sample sizes are similar to those generally employed in the field. Each statistical test was selected based on data distributions using histograms. The variance was generally similar between groups under comparisons. No blinding was performed.

Retrograde and anterograde tracing. For retrograde tracing, adult mice (GAD2-Cre × Rosa-CAG-LSL-tdTomato or SOM-Cre, aged between 93–129 days) were anesthetized with 1–2% isoflurane and scalp was cut open. A small craniotomy (~0.5 mm in diameter) was made over right V1 and retrogradely transported beads (green or red, Lumafluor) were injected using a beveled pipette (~30-µm tip in diameter) backfilled with mineral oil at a speed of ~20 nl min^{-1} (~150–250 µm deep, 1–2 depths, ~100 nl each). Pipettes were left in the brain for additional ~4 min after each injection. Scalp was then closed and general analgesia (buprenorphine, 0.1 mg per kg) was subcutaneously injected. 3 d after the injection, mice were anesthetized with a mixture of ketamine (200 mg per kg) and xylazine (16 mg per kg) and perfused transcardially with phosphate-buffered saline (PBS) and then 4% paraformaldehyde (PFA, wt/vol) in PBS (pH 7.4). The brains were removed and incubated in PFA overnight at 4 °C. The brains were then transferred to 30% sucrose solution (wt/vol) for a few days at 4 °C. Coronal slices (60 µm thick) were cut with a microtome (Thermo Scientific) and mounted on a glass slide (Fisher Scientific) with a mounting medium (Sigma or Vector Laboratories). The brain regions labeled with the beads were identified using an epifluorescence microscope (Axio Zoom.V16 and ApoTome.2, Zeiss) with a mouse brain atlas[56].

For anterograde tracing, mice were perfused as described above after *in vivo* axonal calcium imaging. Coronal brain sections (60 µm thick) were cut and imaged using an epifluorescence microscope (Axio Zoom.V16 and ApoTome.2, Zeiss). Injection sites (RSC) of the virus were confirmed in every mouse studied. No somatic labeling in V1 was detected, indicating that retrograde labeling of V1 neurons by local axonal transduction of the virus in RSC is rare.

Slice preparation and whole-cell recordings for photoactivation of RSC axons *in vitro*. Coronal slices containing the primary visual cortex were prepared from the infected hemispheres (right side) of SOM-Cre mice (aged between 36–49 d, male and female) 18–26 d after the injection of AAV2/1-CAG-ChR2-Venus into RSC. Animals were anesthetized with a mixture of ketamine (200 mg per kg) and xylazine (16 mg per kg) and then perfused transcardially with an ice-cold solution (~20 ml) containing (in mM) 93 *N*-methyl-D-glucamine (NMDG), 2.5 KCl, 1.2 NaH_2PO_4, 30 $NaHCO_3$, 20 HEPES, 25 D-glucose, 5 sodium-ascorbate, 2 thiourea, 3 sodium-pyruvate, 10 $MgSO_4$ and 0.5 $CaCl_2$ with pH adjusted to 7.3 using HCl and bubbled with 95% O_2 and 5% CO_2. Slices (350 µm thick) were cut in the same ice-cold solution using a vibratome (Leica Biosystems) and incubated in the same solution at 34 °C for 10–15 min (protective recovery method[57]).

doi:10.1038/nn.4061

The slices were then moved to artificial cerebrospinal fluid (ACSF) solution containing (in mM) 118 NaCl, 2.5 KCl, 26 $NaHCO_3$, 1.2 NaH_2PO_4, 11 D-glucose, 2 $CaCl_2$ and 1 $MgCl_2$ supplemented with 5 sodium-ascorbate, 2 thiourea, 3 sodium-pyruvate at ~20 °C for at least 1 h.

For recordings, the slices were moved to a recording chamber containing ACSF (not including sodium-ascorbate, thiourea and sodium-pyruvate) maintained at 27 °C. The location of infection in every mouse was inspected in slices with epifluorescence. Pipettes (3–6 MΩ) were filled with low Cl^- internal solution containing (in mM) 122 potassium gluconate, 1 $MgCl_2$, 10 l-glutamic acid-Na, 10 HEPES, 4 Mg-ATP, 0.3 Na-GTP, 10 Na_2-phosphocreatine (pH 7.2, 290 mmol kg^{-1}). L2/3 pyramidal neurons were identified from visual inspection of their morphology and from spiking patterns by current injection. Voltage-clamp recordings were performed at the −60-mV holding potential to readily identify light-evoked excitatory synaptic events as inward currents. The junction potential was not corrected. For ChR2 photoactivation of axons in V1 from RSC, 5-ms 470-nm blue LED pulse (~60 mW) was used ~5 mm from the slice.

Slice preparation and whole-cell recordings for SSFO validation in SOM-INs *in vitro*. For virus infection, neonates (P1) of SOM-Cre mice were anesthetized on ice, placed in a custom-made mold and ~20 nl of AAV2/1-EF1α-DIO-hChR2(C128S/D156A)-EYFP was injected at 2–3 sites in the visual cortex (1.3–1.5 mm lateral and 0 mm anterior to lambda) at 300 μm and 600 μm from the brain surface (~20 nl min^{-1}). Coronal slices containing the primary visual cortex were prepared from the infected hemispheres (right side) (aged between 16–22 d, male and female) 15–21 d after the virus injection. Animals were anesthetized with isoflurane and the brain was removed in an ice-cold solution (~20 ml) containing (in mM) 83 NaCl, 2.5 KCl, 3.3 $MgSO_4$, 1 NaH_2PO_4, 26.2 $NaHCO_3$, 22 D-glucose, 72 sucrose, 0.5 $CaCl_2$ bubbled with 95% O_2 and 5% CO_2. Slices (350 μm thick) were cut in the same ice-cold solution using a vibratome (Leica Biosystems) and incubated in ACSF solution containing (in mM) 118 NaCl, 2.5 KCl, 26 $NaHCO_3$, 1.2 NaH_2PO_4, 11 D-glucose, 2 $CaCl_2$ and 1 $MgCl_2$ at 34 °C for 30 min and then at ~20 °C until used.

For recordings, the slices were moved to a recording chamber containing the same ACSF maintained at 27 °C. Pipettes (2–6 MΩ) were filled with internal solution containing (in mM) 130 potassium gluconate, 5 KCl, 10 HEPES, 2.5 $MgCl_2$, 4 Na_2ATP, 0.4 Na_3GTP, 10 sodium phosphocreatine, 0.6 EGTA (pH 7.2, 290 mmol kg^{-1}). Whole-cell current-clamp recordings were performed from SOM-INs expressing SSFO-EYFP to measure membrane potentials and spikes. For SSFO photoactivation and deactivation, 5-s 470-nm blue LED pulse (~60 mW) and 30-s 590-nm amber LED pulse (~10 mW) were used, respectively, ~5 mm from the slice. SOM-INs with the resting membrane potential above −50 mV were excluded from the analysis.

A **Supplementary Methods Checklist** is available.

51. Brainard, D.H. The Psychophysics Toolbox. *Spat. Vis.* **10**, 433–436 (1997).
52. Pologruto, T.A., Sabatini, B.L. & Svoboda, K. ScanImage: flexible software for operating laser scanning microscopes. *Biomed. Eng. Online* **2**, 13 (2003).
53. Thévenaz, P., Ruttimann, U.E. & Unser, M. A pyramid approach to subpixel registration based on intensity. *IEEE Trans. Image Process.* **7**, 27–41 (1998).
54. Dombeck, D.A., Khabbaz, A.N., Collman, F., Adelman, T.L. & Tank, D.W. Imaging large-scale neural activity with cellular resolution in awake, mobile mice. *Neuron* **56**, 43–57 (2007).
55. Ringach, D.L., Hawken, M.J. & Shapley, R. Dynamics of orientation tuning in macaque primary visual cortex. *Nature* **387**, 281–284 (1997).
56. Paxinos, G. & Franklin, K.B.J. *Paxinos and Franklin's the Mouse Brain in Stereotaxic Coordinates* (Boston: Elsevier/Academic Press, Amsterdam, 2013).
57. Zhao, S. *et al*. Cell type–specific channelrhodopsin-2 transgenic mice for optogenetic dissection of neural circuitry function. *Nat. Methods* **8**, 745–752 (2011).

Erratum: Learning enhances the relative impact of top-down processing in the visual cortex

Hiroshi Makino & Takaki Komiyama
***Nat. Neurosci.*; doi:10.1038/nn.4061; corrected online 16 July 2015**

In the version of this article initially published online, the Acknowledgments listed T.K. as a recipient of the Robertson Stem Cell Prize from the New York Stem Cell Foundation. This should have read a NYSCF-Robertson Investigator. The error has been corrected for the print, PDF and HTML versions of this article.